800-fs, 330-μJ pulses from a 100-W regenerative Yb:YAG thin-disk amplifier at 300 kHz and THz generation in $LiNbO_3$

W. Schneider,[1,2] A. Ryabov,[1,2] Cs. Lombosi,[3] T. Metzger,[4] Zs. Major,[1,2] J. A. Fülöp,[5,6] and P. Baum[1,2,*]

[1]*Ludwig-Maximilians-Universität München, Am Coulombwall 1, 85748 Garching, Germany*

[2]*Max-Planck-Institute of Quantum Optics, Hans-Kopfermann-Str. 1, 85748 Garching, Germany*

[3]*Institute of Physics and Szentágothai Research Centre, University of Pécs, Ifjúság ú. 6 and 20, 7624 Pécs, Hungary*

[4]*TRUMPF Scientific Lasers GmbH + Co. KG, Feringastr. 10a, 85774 Unterföhring, Germany*

[5]*MTA-PTE High-Field Terahertz Research Group, Ifjúság ú. 6, 7624 Pécs, Hungary*

[6]*ELI-ALPS, ELI-Hu Nkft., Dugonics tér 13, 6720 Szeged, Hungary*

**Corresponding author: peter.baum@lmu.de*

Received September 5, 2014; revised October 15, 2014; accepted October 17, 2014;
posted October 20, 2014 (Doc. ID 222516); published November 18, 2014

Yb:YAG thin-disk lasers offer extraordinary output power, but systems delivering femtosecond pulses at a repetition rate of hundreds of kilohertz are scarce, even though this regime is ideal for ultrafast electron diffraction, coincidence imaging, attosecond science, and terahertz (THz) spectroscopy. Here we describe a regenerative Yb:YAG amplifier based on thin-disk technology, producing 800-fs pulses at a repetition rate adjustable between 50 and 400 kHz. The key design elements are a short regenerative cavity and fast-switching Pockels cell. The average output power is 130 W before the compressor and 100 W after compression, which at 300 kHz corresponds to pulse energies of 430 and 330 μJ, respectively. This is sufficient for a wide range of nonlinear conversions and broadening/compression schemes. As a first application, we use optical rectification in $LiNbO_3$ to produce 30-nJ single-cycle THz pulses with 6 W pump power. The electric field exceeds 10 kV/cm at a central frequency of 0.3 THz, suitable for driving structural dynamics or controlling electron beams.

OCIS codes: (140.7090) Ultrafast lasers; (160.3730) Lithium niobate; (190.7110) Ultrafast nonlinear optics.
http://dx.doi.org/10.1364/OL.39.006604

Femtosecond lasers are indispensable in many fields of science and technology. While Ti:sapphire-based sources typically produce the shortest pulses, there is a recent paradigm shift to Yb:YAG technology [1], offering significantly higher output power and scalability, especially in geometries with thin disks, slabs, or fibers. Reported Yb:YAG-based lasers producing femtosecond pulses (<1 ps) can be sorted into mode-locked oscillators [2,3], fiber lasers [4,5], long-cavity oscillators [6–8], slab amplifiers [9,10], disk amplifiers [11,12], or cascaded laser chains for pulses in the multi-mJ regime [13–18].

Many applications require repetition rates between 100 kHz and 1 MHz. This intermediate regime between oscillators and conventional amplifiers is unusual, but beneficial in pump-probe spectroscopy, material processing, attosecond science, or coincidence imaging, for improving the signal-to-noise ratio, enhancing the total flux or reducing acquisition times. Our particular case is ultrafast electron diffraction with single-electron pulses [19,20] for probing structural dynamics with atomic resolution in space and time [21]. An optimum repetition rate is 200–300 kHz [22]; yet the laser pulses should be powerful enough (hundreds of μJ) for effective nonlinear optical frequency conversions to the ultraviolet/visible/infrared [23,24] and THz domains [25,26], in order to initiate and control atomic-scale dynamics.

None of the Yb:YAG-based laser systems demonstrated so far (fiber, slab, crystal, disk) [1], provide sufficiently intense and stable femtosecond pulses at hundreds of kHz for these diffraction applications, which require maximum simplicity of the laser system. Hence, we describe here the design and operation of a regenerative Yb:YAG amplifier based on thin-disk technology, producing 800-fs pulses at an adjustable repetition rate between 50 and 400 kHz.

Figure 1 depicts the experiment, based on a preliminary attempt [27]. The seed (t-Pulse 50, Amplitude Systèmes) is a mode-locked Yb:YAG oscillator with a repetition rate of 50 MHz at a central wavelength of 1030 nm, delivering fs pulses with an energy of ~40 nJ and a spectral bandwidth of 2.7 nm. These pulses propagate through transmission gratings with 1,400 lines per mm and $f = 1\,\mathrm{m}$ lenses, producing a group-velocity dispersion of 27 ps^2 and ~160-ps pulses for chirped-pulse amplification.

The desired high repetition rate in the multi-hundred-kHz regime together with the thin-disk's limited gain per reflection of ~10% puts some significant constraints on

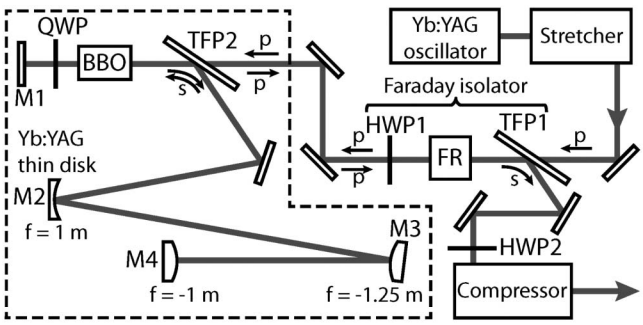

Fig. 1. Experimental setup and optical layout of the regenerative amplifier. TFP, thin-film polarizer; FR, Faraday rotator; HWP, half-wave plate; BBO, Pockels cell, QWP, quarter-wave plate; M1–M4, mirrors. The regenerative amplifier cavity is marked with a dashed line. Arrows denote the polarization state.

the regenerative cavity. Each amplified pulse must leave the cavity before the next seed pulse can enter. For a design at $\nu_{rep} = 400$ kHz and 10% gain, we estimate that $N_{gain} \approx 200$ round trips are required. Hence the maximum cavity length is $c/(2\nu_{rep}N_{gain}) \approx 1.9$ m and the switching time for coupling the pulses in and out must be shorter than $1/(\nu_{rep}N_{gain}) \approx 12$ ns. This necessitates a small Pockels cell crystal to minimize the high voltage required for switching. In turn, the cavity mode must be designed small enough to avoid clipping and damage, but also large enough to minimize B-integral accumulation.

Our design is depicted in Fig. 1 within the dashed outline. The disk module (TRUMPF) employs a ~1/10-mm-thick, ~10%-doped Yb:YAG thin-disk on a water-cooled heat sink, pumped by laser diodes at ~940 nm (LDM 500, Laserline GmbH). The disk has a radius of curvature of $r \approx 2$ m (M2). In order to comply with the considerations above, we use two convex mirrors (M3, M4) and a total cavity length of 1670 mm. The cavity's stability is calculated using ray transfer matrices (see Fig. 2). The beam diameter in the Pockels cell is <1.5 mm (full width at half-maximum), and the accumulated B-integral is ~0.05. The Pockels cell is an anti-reflection-coated BBO crystal with a size of 6 mm × 6 mm × 25 mm, driven with a rise time of ~6 ns by a pulsed high-voltage supply (Bergmann KG). Hence we conform to all considerations outlined above.

A mode-matching telescope is used to couple in the seed pulses with a typical switching sequence [28]: a thin-film polarizer (TFP-1), Faraday rotator (FR), and half-wave plate (HWP) form an isolator. P-polarized incoming pulses enter the amplifier cavity through a thin-film polarizer (TFP-2). The Pockels cell (BBO) is in its "off" switching state, and a double-pass through a quarter-wave plate (QWP) produces back-propagating pulses with s-polarization, which are reflected by TPF-2. Before their return from mirror M4, the Pockels cell is switched "on", rotating polarization by 45° and rendering the QWP ineffective. S-polarized pulses are therefore captured in the amplifier cavity until the Pockels cell is switched "off" again. The QWP produces p-polarization, and the pulses leave the cavity through TFP-2. The Faraday isolator directs them toward compression and applications.

In the following, we applied 120 round trips at 300 kHz before coupling the final pulse out of the amplifier cavity. More round trips could destroy the Pockels cell, as described in more detail below. Figure 3(a) shows the increase of output power with increasing pump power. Ellipticity, observed after the end mirror M1, increases

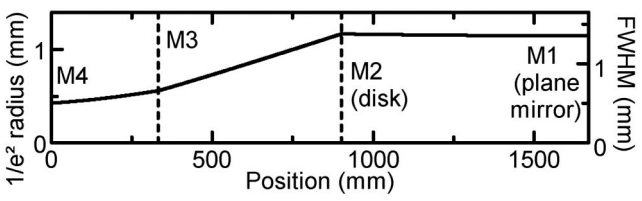

Fig. 2. Design of the length-limited amplifier cavity (dashed area in Fig. 1) for operation at high repetition rates up to 400 kHz. Solid, beam diameter along the cavity mode; dashed, position of mirrors M2 and M3. FWHM, full width at half-maximum.

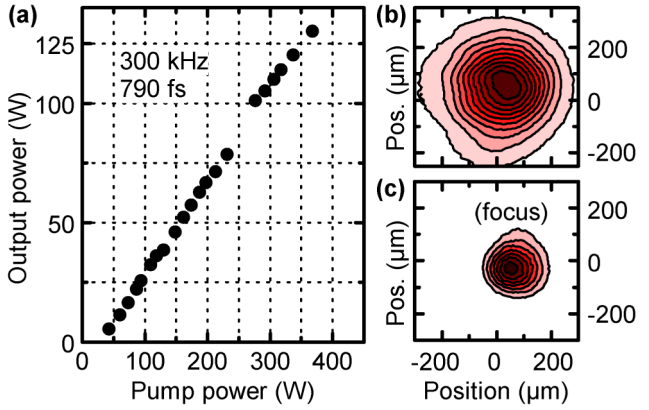

Fig. 3. Output performance. (a) Output power in dependence of the pump power. (b) Beam profile after a focus. (c) Shape of a focused spot. Intensity of the beam profiles is normalized.

slightly from 0.95 at low power up to 0.8 at above 100 W of output. Nevertheless, the cavity is always stable. At 370 W of pump power, we achieve an output power of 130 W before the compressor. This corresponds to a pulse energy of 430 μJ. Figures 3(b) and 3(c) show the beam profiles at 130 W measured after the focus and in the focus of an $f = 450$ mm lens, respectively. The measured M^2 value at an output of 130 W is 1.30 and 1.35 for the horizontal and the vertical directions, respectively.

Compression of the 130-W output pulses is achieved using two reflective gratings with 1400 lines per mm at a separation of 1.76 m; the angle of incidence is 47°. The throughput of this compressor amounts to 77%; ~100 W are emitted for applications. Figure 4 shows the spectrum and autocorrelation trace (pulseCheck, APE GmbH). With respect to the seed spectrum with a width of 2.7 nm, the amplified spectrum shows signs of gain narrowing and a width of 2.3 nm. Still, the Fourier limit calculated from the measured spectrum is 740 fs. There is no evidence for self-phase modulation or any other nonlinear processes; the slight wiggles are interferences at the spectrometer's fiber entrance. The autocorrelation trace indicates compressed pulses of 790 fs duration, assuming a sech^2 shape. This is within 7% of the Fourier limit and indicates a good match between stretcher, intra-cavity dispersion, and compressor in our system. Higher order chirp, as can occur from self-phase modulation, is negligible.

The output power is stable to about 1% rms on the sub-minute time scale. On longer time scales, there are some systematic oscillations of ±2% (peak-to-peak) caused by

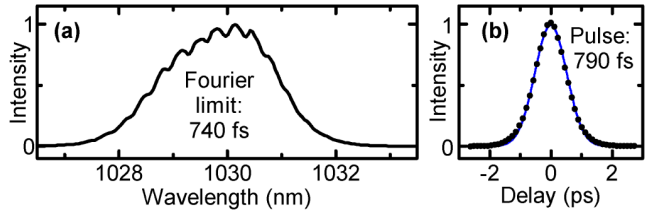

Fig. 4. Regenerative amplifier performance in the frequency and time domains. (a) Output spectrum. (b) Autocorrelation trace (black dots), fitted assuming a sech^2-shaped temporal pulse profile (blue line). The pulse duration (790 fs) is close to the measured spectrum's Fourier limit (740 fs).

the disk's chiller system, which is currently only stable to ±1 K. The laser reliably runs over several days without alignment; no significant drifts of output power are observable (<0.8% over a day, <0.05% per hour).

We note in Fig. 3(a) the almost linear relation; we do not reach saturation. This suggests that we could further increase the pump power or the number of round trips and achieve even higher output and stability. In practice, however, this is limited by Pockels cell damage, occurring either at the front or back surface as an extended dark region around the center, where the beam passes through. We attribute this damage to the effects of average intra-cavity power in conjunction with coating imperfections. One solution would be to obtain better-coated crystals, which is technologically challenging. An alternative would be to redesign the cavity for a slightly larger mode at the Pockels cell crystal, accepting some minor clipping. There is also room for moderate lengthening of the cavity, especially if more intense seed pulses are applied at a reduced number of round trips. In view of these options, and potentially others, it might be possible to further scale our 300-kHz regenerative disk amplifier concept toward higher output powers, in case this should be desirable.

As a first application, we produced THz radiation by optical rectification in 0.6% MgO-doped stoichiometric lithium niobate ($LiNbO_3$) using tilted-pulse-front pumping [29]. For safety, in order to avoid excessive average powers, we reduced the laser's repetition rate to 50 kHz for these experiments. Tilted pulses were generated with a 400-lines-per-mm gold grating and an imaging lens with $f \approx 150$ mm placed at a distance of 1750 mm after the grating. The front surface of the $LiNbO_3$ crystal was placed 166 mm after the imaging lens. This produced a large demagnification ratio of about 1:10, which was necessary to compensate for the significantly different damage thresholds of the grating and the $LiNbO_3$ crystal, measured with our system at 300 kHz as ~0.7 GW/cm^2 and ~110 GW/cm^2 peak intensity, respectively. Crystal damage was probably due to heating and the related thermo-optic effect. We note that a demagnification of about 1:2 would have been ideal to minimize the imaging distortions [30], but this was not critical for our small excited area at the $LiNbO_3$ crystal (see below). Incidence and exit angles at the grating approximated the ideal case, minimizing temporal distortions [31].

The pump spot size at the position of the $LiNbO_3$ prism was 710 μm × 670 μm (horizontal × vertical, full width at half-maximum). Laser polarization was set with a half-wave plate along $LiNbO_3$'s z-axis, parallel to the axis of pulse-front tilt. The THz radiation from the prism's exit face, cut at 63°, was observed with a pyroelectric detector (Gentec-EO). With knife-edge scans, we determined the effective size of the THz-emitting area as 1560 μm × 670 μm (horizontal × vertical, full width at half-maximum). This is close to the expected value, considering the 63° emission angle. Using beam-profile scans at different distances, we determined the divergence of the THz radiation to 18° horizontally and 40° vertically (full width at half-maximum). This asymmetry and magnitude are expected from the elongated emission area with dimensions close to the THz wavelength. The input beam's cross-section could be shaped with cylindrical optics if a more round and uniformly divergent THz beam is required.

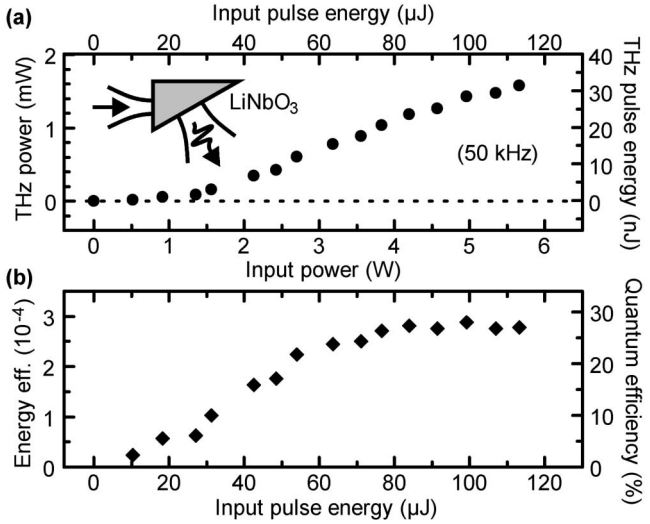

Fig. 5. Performance of the THz generation with tilted pulses in $LiNbO_3$. (a) Output power and THz pulse energy in dependence of the input power and pulse energy. (b) Quantum efficiency and energy-conversion efficiency.

The power of the emitted THz radiation (outside of $LiNbO_3$) versus the laser power (transmitted into $LiNbO_3$) is depicted in Fig. 5(a). At low energy, there is an almost quadratic dependence; at higher energy a more linear relation indicates the onset of saturation. We stopped this study at ~6 W pump power or 120 μJ pulse energy, in order not to risk damage of the $LiNbO_3$ prism, which was not cooled or specially mounted. Nevertheless, the measured THz output power was 1.6 mW. This corresponds to 30 nJ pulse energy, 2.8×10^{-4} pump-to-THz conversion efficiency and close to 30% quantum efficiency. This efficiency, similar to earlier results [32], can be increased further by increasing the beam diameter in the horizontal direction to enable larger interaction length or by using shorter pump pulses [30,33], but pump-THz walk-off must be considered.

Electro-optical sampling in a 300-μm-thick GaP crystal revealed the time-dependent electric field of the THz pulses; see Fig. 6(a). The single-cycle pulse had a peak field strength of about 11 kV/cm, determined from the electro-optical coefficients of GaP [34]. The corresponding spectral amplitude is depicted in Fig. 6(b), revealing a center at 0.3 THz. These pulses have an attractive combination of repetition rate, field strengths and central

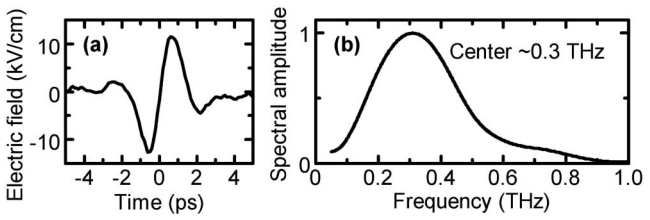

Fig. 6. Characterization of the THz pulses. (a) Time-dependent electric field of the THz pulses with peak strength of ~11 kV/cm. (b) THz spectrum at full output power (spectral amplitude).

frequency for driving structural motion in materials or for accelerating/controlling electron beams.

Assuming that the thermal load on the $LiNbO_3$ prism can be handled by appropriate cooling and mounting, which remains to be proven in the experiment, we can extrapolate our results to a scenario where our laser's full output power at 300 kHz is applied for THz generation. Referring to Fig. 5(b), we assume that the regime of constant quantum efficiency, i.e., linear energy scaling, continues beyond the 120 μJ applied so far. Using the full 330 μJ available at 300 kHz and 100 W, we would then obtain a THz output power of about 25 mW and about 85 nJ per pulse. Electric fields could be increased by tighter focusing or field enhancement at microstructures.

In conclusion, the here reported high-power Yb:YAG laser source produces femtosecond pulses with hundreds-of-μJ energy at an adjustable repetition rate of 50–300 kHz, probably up to 400 kHz if desirable. The peak power of the cycle-averaged intensity distribution of the 800-fs pulses is 400 MW. The pulses could be further shortened by driving the amplifier in the regime of self-phase modulation [11], by shaping the seed spectrum [15], by controlling the gain spectrum [28], or by nonlinear broadening/compression [35–37]. The ability to efficiently produce intense THz radiation at 50 kHz demonstrates the suitability of our thin-disk laser for advanced nonlinear frequency conversions at optimum repetition rates for ultrafast electron diffraction, attosecond/femtosecond spectroscopy, or coincidence imaging of molecular dynamics.

We acknowledge funding from ERC ("4D imaging"), from Munich-Centre of Advanced Photonics, from IMPRS of Advanced Photon Science, and from BMBF contract 13N12082. J. A. F. acknowledges support from János Bolyai Research Scholarship (Hungarian Academy of Sciences) and OTKA grants 101846 and 113083. We thank Roswitha Graf for her contributions at the initial stage of this project and J. Hebling for helpful discussion.

References

1. H. Fattahi, H. G. Barros, M. Gorjan, T. Nubbemeyer, B. Alsaif, C. Y. Teisset, M. Schultze, S. Prinz, M. Haefner, M. Ueffing, A. Alismail, L. Vámos, A. Schwarz, O. Pronin, J. Brons, X. T. Geng, G. Arisholm, M. Ciappina, V. S. Yakovlev, D.-E. Kim, A. M. Azzeer, N. Karpowicz, D. Sutter, Z. Major, T. Metzger, and F. Krausz, Optica **1**, 45 (2014).
2. O. Pronin, J. Brons, C. Grasse, V. Pervak, G. Boehm, M.-C. Amann, V. L. Kalashnikov, A. Apolonski, and F. Krausz, Opt. Lett. **36**, 4746 (2011).
3. C. J. Saraceno, F. Emaury, O. H. Heckl, C. R. E. Baer, M. Hoffmann, C. Schriber, M. Golling, T. Suedmeyer, and U. Keller, Opt. Express **20**, 23535 (2012).
4. T. Eidam, S. Hanf, E. Seise, T. V. Andersen, T. Gabler, C. Wirth, T. Schreiber, J. Limpert, and A. Tünnermann, Opt. Lett. **35**, 94 (2010).
5. A. Klenke, S. Breitkopf, M. Kienel, T. Gottschall, T. Eidam, S. Haedrich, J. Rothhardt, J. Limpert, and A. Tuennermann, Opt. Lett. **38**, 2283 (2013).
6. S. V. Marchese, C. R. E. Baer, A. G. Engqvist, S. Hashimoto, D. J. H. C. Maas, M. Golling, T. Suedmeyer, and U. Keller, Opt. Express **16**, 6397 (2008).
7. D. Bauer, I. Zawischa, D. Sutter, A. Killi, and T. Dekorsy, Opt. Express **20**, 9698 (2012).
8. C. J. Saraceno, F. Emaury, C. Schriber, M. Hoffmann, M. Golling, T. Südmeyer, and U. Keller, Opt. Lett. **39**, 9 (2014).
9. P. Russbueldt, T. Mans, G. Rotarius, J. Weitenberg, H. D. Hoffmann, and R. Poprawe, Opt. Express **17**, 12230 (2009).
10. P. Russbueldt, T. Mans, J. Weitenberg, H. D. Hoffmann, and R. Poprawe, Opt. Lett. **35**, 4169 (2010).
11. R. Fleischhaker, R. Gebs, A. Budnicki, M. Wolf, J. Kleinbauer, and D. Sutter, in *Conference on Lasers and Electro-Optics Europe (CLEO)* (IEEE, 2013), p. 1.
12. C. Teisset, M. Schultze, R. Bessing, M. Haefner, S. Prinz, D. Sutter, and T. Metzger, in *Advanced Solid-State Lasers Congress Postdeadline* (Optical Society of America, 2013), paper JTh5A.1.
13. K.-H. Hong, J. T. Gopinath, D. Rand, A. M. Siddiqui, S.-W. Huang, E. Li, B. J. Eggleton, J. D. Hybl, T. Y. Fan, and F. X. Kärtner, Opt. Lett. **35**, 1752 (2010).
14. M. Schulz, R. Riedel, A. Willner, T. Mans, C. Schnitzler, P. Russbueldt, J. Dolkemeyer, E. Seise, T. Gottschall, S. Hadrich, S. Duesterer, H. Schlarb, J. Feldhaus, J. Limpert, B. Faatz, A. Tunnermann, J. Rossbach, M. Drescher, and F. Tavella, Opt. Lett. **36**, 2456 (2011).
15. S. Klingebiel, C. Wandt, C. Skrobol, I. Ahmad, S. A. Trushin, Z. Major, F. Krausz, and S. Karsch, Opt. Express **19**, 5357 (2011).
16. M. Schulz, R. Riedel, A. Willner, S. Düsterer, M. J. Prandolini, J. Feldhaus, B. Faatz, J. Rossbach, M. Drescher, and F. Tavella, Opt. Express **20**, 5038 (2012).
17. J.-P. Negel, A. Voss, M. A. Ahmed, D. Bauer, D. Sutter, A. Killi, and T. Graf, Opt. Lett. **38**, 5442 (2013).
18. J. Tuemmler, R. Jung, H. Stiel, P. V. Nickles, and W. Sandner, Opt. Lett. **34**, 1378 (2009).
19. A. H. Zewail, Science **328**, 187 (2010).
20. P. Baum, Chem. Phys. **423**, 55 (2013).
21. P. Baum, J. Phys. B **47**, 124005 (2014).
22. S. Lahme, C. Kealhofer, F. Krausz, and P. Baum, Struct. Dyn. **1**, 034303 (2014).
23. C. Homann, C. Schriever, P. Baum, and E. Riedle, Opt. Express **16**, 5746 (2008).
24. M. Bradler, C. Homann, and E. Riedle, Appl. Phys. B **113**, 19 (2013).
25. J. Hebling, K.-L. Yeh, M. C. Hoffmann, and K. A. Nelson, IEEE J. Sel. Topics Quantum Electron. **14**, 345 (2008).
26. H. Hirori and K. Tanaka, IEEE J. Sel. Topics Quantum Electron **19**, 8401110 (2013).
27. R. Graf, T. Metzger, M. Chyla, D. Sutter, Z. Major, A. Apolonski, and F. Krausz, *Europhoton Conference* (2012), paper POSD.2.
28. W. Koechner, *Solid-State Laser Engineering* (Springer, 2006).
29. J. Hebling, G. Almasi, I. Z. Kozma, and J. Kuhl, Opt. Express **10**, 1161 (2002).
30. J. A. Fülöp, L. Palfalvi, G. Almasi, and J. Hebling, Opt. Express **18**, 12311 (2010).
31. D. Kreier and P. Baum, Opt. Lett. **37**, 2373 (2012).
32. M. C. Hoffmann, K.-L. Yeh, J. Hebling, and K. A. Nelson, Opt. Express **15**, 11706 (2007).
33. J. A. Fülöp, L. Palfalvi, M. C. Hoffmann, and J. Hebling, Opt. Express **19**, 15090 (2011).
34. X. C. Zhang and J. Xu, *Introduction to THz Wave Photonics* (Springer, 2010).
35. S. Haedrich, A. Klenke, A. Hoffmann, T. Eidam, T. Gottschall, J. Rothhardt, J. Limpert, and A. Tuennermann, Opt. Lett. **38**, 3866 (2013).
36. F. Emaury, C. F. Dutin, C. J. Saraceno, M. Trant, O. H. Heckl, Y. Y. Wang, C. Schriber, F. Gerome, T. Sudmeyer, F. Benabid, and U. Keller, Opt. Lett. **21**, 4986 (2013).
37. Y. Y. Wang, X. Peng, M. Alharbi, C. F. Dutin, T. D. Bradley, F. Gerome, M. Mielke, T. Booth, and F. Benabid, Opt. Lett. **37**, 3111 (2012).